Article

Discovery Medicine 2026; 38(212): 2853–2865
https://doi.org/10.24976/Discov.Med.202638212.220

HDAC11 and COMP Modulate Breast Cancer Cell Phenotypes and Osteoclastogenic Responses in a Co-culture Model

Xiaohong Yang[1,†], Ping Wang[2,†], Yong Ping[3], Guan Lv[1], Yan Zhang[4,*]

[1]Department of Thyroid and Breast Surgery, Nanjing Gaochun People's Hospital, 211300 Nanjing, Jiangsu, China
[2]Department of Endocrinology, Nanjing Gaochun People's Hospital, 211300 Nanjing, Jiangsu, China
[3]Department of Orthopedics, Rizhao Central Hospital, 276800 Rizhao, Shandong, China
[4]Department of Cardiovascular Research, Shinshu University School of Medicine, 390-8621 Matsumoto, Japan
*Correspondence: yan_zhang0916@163.com (Yan Zhang)
[†]These authors contributed equally.
Submitted: 9 April 2026 Revised: 30 June 2026 Accepted: 25 August 2026 Published: 23 September 2026

Background: Cartilage oligomeric matrix protein (COMP) interacts with stromal interaction molecule 1 (STIM1). Both COMP and histone deacetylase 11 (HDAC11) are highly expressed in breast cancer cells (BCC). Given the reported inhibitory effect of HDAC3 on COMP acetylation, HDAC11 may be associated with the regulation of COMP acetylation in BCC. Therefore, this study investigated the association between HDAC11, COMP, and osteoclast-related responses in breast cancer (BC) using a co-culture model, providing *in vitro* correlative evidence that may be relevant to the pathophysiology of bone metastasis.
Methods: Bioinformatics analyses verified HDAC11/COMP expression and their correlation in invasive BC. HDAC11 and COMP expressions were manipulated in MCF-7/MDA-MB-231 cells, and then cells were co-cultured with RAW264.7 macrophages to mimic the bone microenvironment. Co-IP and *in vitro* acetylation assays were conducted to clarify HDAC11-COMP interaction and the association between HDAC11 knockdown and COMP acetylation levels. Functional, molecular detection and microspectrofluorometry assays were performed to assess BCC malignant phenotypes, osteoclast biological behaviors, HDAC11/COMP/STIM1 expression and intracellular Fura-2 signals.
Results: HDAC11 and COMP levels were markedly upregulated and positively correlated in invasive BC ($p < 0.05$). HDAC11 overexpression boosted BCC viability, migration, invasion and COMP expression, while HDAC11 knockdown had the opposite effects and elevated COMP acetylation ($p < 0.05$). In the BCC-RAW264.7 co-culture system, HDAC11 knockdown suppressed the maintenance, survival and functional activity of differentiated osteoclast-like cells, bone resorption, STIM1 expression and Fura-2 signals in the co-cultured cell population ($p < 0.001$). Moreover, COMP overexpression reversed the inhibitory effects of HDAC11 knockdown on BCC malignant phenotypes, osteoclast activation, STIM1 expression and Fura-2 ratio signals ($p < 0.01$).
Conclusion: HDAC11 knockdown is associated with increased acetylated lysine signals in COMP immunoprecipitates, along with changes in STIM1 protein abundance and Fura-2 signals in the co-culture system. Collectively, these findings reveal a correlation between HDAC11, COMP and the regulation of both BCC progression and osteoclastogenic activity, providing a basis for future *in vivo* studies to investigate its potential role in BC bone metastasis.

Keywords: HDAC11; bone metastasis; breast cancer; COMP; STIM1; acetylation

Introduction

Breast cancer (BC) is currently the most serious health threat to women worldwide [1,2,3]. BC bone metastasis, a frequent and severe complication of advanced BC, significantly worsens prognosis, reduces quality of life, and remains a major clinical challenge [4,5]. Consequently, elucidating the mechanisms underlying BC bone metastasis is of critical importance for identifying effective therapeutic targets.

Previous studies have established that, in BC bone metastasis, breast cancer cells (BCCs) and osteoclasts mutually interact to form a vicious cycle within the bone microenvironment. Osteoclasts are responsible for the resorption of old bone and thus contribute to maintaining bone mass stability [6,7,8]. BCCs secrete various cytokines that promote osteoclast differentiation and maturation, while activated osteoclasts resorb bone and release growth factors that further enhance BCC proliferation and survival [9,10,11,12]. Therefore, disrupting this vicious cycle by targeting osteoclasts represents a major therapeutic strategy for preventing bone metastasis in BC.

Calcium ion (Ca^{2+}) plays a significant role in regulating osteoclast differentiation and function [13]. Store-operated Ca^{2+} entry (SOCE) is a common Ca^{2+} signal-

ing pathway activated by Ca^{2+} depletion or reduction from endoplasmic reticulum, thereby resulting in Ca^{2+} influx [14,15,16]. Numerous studies have verified that stromal interaction molecule (STIM) proteins, especially STIM1, mediate SOCE [17,18]. Accordingly, we hypothesized that a substance secreted by BCC could stimulate osteoclasts to activate the Ca^{2+} signaling pathway. Interestingly, cartilage oligomeric matrix protein (COMP) has been identified as a STIM1-interacting protein and is highly expressed in the blood of BC patients [19,20]. Hence, we inferred that COMP, through its interaction with STIM1, may influence Fura-2 signaling and osteoclast function, which may be relevant to the pathophysiology of BC bone metastasis.

Furthermore, histone acetylation modifications are regulated by histone deacetylase (HDAC) and histone acetyltransferase (HAT) and have been shown to greatly affect the functions of various cell types [21,22,23]. Existing evidence has revealed that HDAC3 inhibits COMP acetylation [24]. Using GEPIA to analyze the expression of various HDACs (HDAC1-11) in BC, we found that HDAC11 was the only HDAC significantly overexpressed in tumor tissues. However, limited studies have investigated the functional significance of HDAC11 in BC. In this study, we explored the association among HDAC11, COMP, and STIM1-related protein abundance in BC, as well as their collective effects on cell phenotypes and osteoclastogenic responses *in vitro*, which may provide insights into breast cancer biology relevant to bone metastasis.

Materials and Methods

Bioinformatics Analysis

The expression data ofHDAC11 and COMP in BC (n = 1085) and normal tissue (n = 291) samples were obtained from gene expression profiling interactive analysis 2 (http://gepia2.cancer-pku.cn/#index) to analyze their expression levels in BC. Meanwhile, the correlation between HDAC11 and COMP expression in BC was analyzed using StarBase (https://rna.sysu.edu.cn/encori/) with Pearson's correlation coefficient. Pearson correlation analysis of continuous gene expression data was automatically performed by the StarBase platform. The correlation coefficient (r) and *p*-value were extracted directly from the online analysis output.

Cell Culture

Human BCC lines MCF-7 (HTB-22) and MDA-MB-231 (CRM-HTB-26), MCF-10A and macrophages RAW264.7 (TIB-71) (ATCC, Manassas, VA, USA) were cultured in complete Dulbecco's Modified Eagle's Medium (DMEM; 10-014-CV, Corning Inc., Corning, NY, USA) supplemented with 10% fetal bovine serum (FBS, S9030, Solarbio, Beijing, China). Cells were incubated at 37 °C in a 5% CO_2 incubator. All cell lines were authenticated by short tandem repeat (STR) profiling, confirming a full match with the standard genotypes of the corresponding cell lines, and were certified negative for mycoplasma contamination, thereby meeting all experimental requirements.

Cell Transfection

The sequences of HDAC11 and COMP were cloned into pcDNA3.1 vectors (BR039, Fenghui Biotechnology, Changsha, China) to generate the corresponding overexpression plasmids, and their negative controls (NC) were provided by GenePharma (Shanghai, China). GenePharma (Shanghai, China) also synthesized short hairpin RNA targeting HDAC11 (shHDAC11, 5'-GTTTCTGTTTGAGCGTGTGGA-3') and shNC (5'-TTCTCCGAACGTGTCACGT-3) by cloning the corresponding sequences into the pLKO.1 vector backbone. MCF-7 and MDA-MB-231 cells were transfected with shHDAC11/shNC alone or in combination with COMP overexpression plasmids/NC using Lipofectamine 3000 (L3000015, Invitrogen, Carlsbad, CA, USA). For transfection, 100 ng of plasmids (HDAC11 or COMP overexpression plasmids/NC) or 100 ng of shRNA (shHDAC11/shNC) plasmid constructs were transfected into MCF-7/MDA-MB-231 cells using Lipofectamine 3000 (L3000015, Invitrogen, Carlsbad, CA, USA) according to the manufacturer's instructions, resulting in a final plasmid concentration of 1 μg/mL in the culture medium. ShHDAC11, HDAC11 and COMP overexpression plasmids, and Lipofectamine^{TM} 3000 were diluted in Opti-MEM (31985062, Thermo Fisher Scientific, Waltham, MA, USA) with P3000^{TM} reagent and then incubated at 37 °C for 15 min. MDA-MB-231/MCF-7 cells (1×10^4 cells/well) were seeded in 96-well plates and grown to 90% confluence. The gene-lipid complexes were then incubated with the cells for 48 h at 37 °C.

Co-Immunoprecipitation (Co-IP)

Interaction between HDAC11 and COMP was evaluated by Co-IP assay using a Co-IP kit (abs955, Absin, Shanghai, China). First, MCF-7/MDA-MB-231 cell lysates were prepared using lysis buffer according to the manufacturer's protocol. Subsequently, 500 μL of cell lysate was incubated with 5 μg of anti-HDAC11 antibody (ab246512, Abcam, UK) for HDAC11 immunoprecipitation, 5 μg of anti-COMP antibody (ab260037, Abcam, UK) for COMP immunoprecipitation or normal rabbit IgG (ab172730, Abcam, Cambridge, UK) for 1 h at 4 °C. Protein A (5 μL) and Protein G (5 μL) were then added to the cell lysate, followed by incubation for 3-h and centrifugation at 12,000 ×g for 1-min. The beads were washed 5 times with 0.5 mL of Wash buffer (with gentle inversion followed by centrifugation at 2500 ×g for 2 min after each wash). Finally, bound proteins were eluted with 2× SDS loading buffer by boiling at 95 °C for 10 min, followed by western blot analysis.

Acetylation Assays In Vitro

The effect of HDAC11 on COMP acetylation was assessed by *in vitro* acetylation assays, as described in a

previous study [25]. Briefly, MCF-7/MDA-MB-231 cells were transfected with shHDAC11/shNC and glutathione S-transferase-fused COMP. Subsequently, the cells were incubated with a reaction mixture containing acetyltransferase assay buffer (50 µL, orb608458, Biorbyt, Cambridge, UK), acetyl-CoA (20 µM, A8070, Solarbio, Beijing, China), 1 mM dithiothreitol (DTT, R0861, Solarbio, Beijing, China), 50 mM Tris-Cl (pH 8.0, T1150, Solarbio, China), 0.1 mM EDTA (E1170, Solarbio, Beijing, China), and 5% glycerol (G8190, Solarbio, Beijing, China) at 30 °C for 2 h. The reaction mixture was then analyzed by sodium dodecyl sulfate polyacrylamide gel electrophoresis (SDS-PAGE, P0678, Beyotime, Shanghai, China), followed by western blot analysis.

Osteoclastogenesis Assay In Vitro and Cell Co-Culture

RAW264.7 cells (3×10^3 cells/well) were cultured in 96-well plates and incubated overnight. Subsequently, the cells were exposed to 50 ng/mL of receptor activator of nuclear factor-kappa B ligand (RANKL) for 7 days to induce differentiation into mature osteoclasts, as confirmed by TRAP staining and the presence of multinucleated cells (≥3 nuclei), and were then cultured overnight in 96-well plates for subsequent co-culture. After transfection with shHDAC11 and/or COMP/HDAC11 overexpression plasmids, MCF-7/MDA-MB-231 cells (1×10^3 cells/well) were added to each well and co-cultured with RAW264.7 cells for 7 days to evaluate the effects of BCCs on osteoclast function [26]. Afterward, less adherent macrophages were gently detached from the adherent cancer cells by pipetting. The detached macrophages were collected from the culture medium, whereas the adherent cancer cells were trypsinized and collected separately. For Western blot and qRT-PCR analyses, total protein and RNA were extracted from the separated cell populations (macrophages or cancer cells) collected as described above. For TRAP staining and Fura-2 microspectrofluorometry, assays were performed directly on the mixed co-cultured cell population without separation.

Quantitative Real-Time Reverse Transcription Polymerase Chain Reaction (qRT-PCR)

Total RNA was extracted from transfected MCF-7/MDA-MB-231 cells using the RNeasy Mini Kit (74104, Qiagen, Hilden, Germany) and reverse-transcribed into complementary DNA using the PrimeScriptTM RT Reagent Kit (RR037A, TaKaRa, Beijing, China). qRT-PCR was performed on an ABI 7500 System (Thermo Fisher Scientific, Waltham, MA, USA) using 2× SYBR Green qPCR Master Mix (B21203, Bimake, Houston, TX, USA) under the following conditions: 40 cycles of 95 °C for 15 s, 55 °C for 30 s, and 72 °C for 30 s. HDAC11 and COMP expression levels were normalized to the internal control glyceraldehyde 3-phosphate dehydrogenase (GAPDH), and relative expression was calculated using the $2^{-\Delta\Delta Ct}$ method [27]. The PCR sequences (Sangon, Shanghai, China) were as follows: HDAC11 (forward, 5'-GGGATGCTACACACAACCCA-3'; reverse, 5'-CAGCAAAGGACCACTTGAGC-3'), COMP (forward, 5'-CCGAGTCCGCTGTATCAACA-3'; reverse, 5'-TATGTTGCCCGGTCTCACAC-3'), GAPDH (forward, 5'-AATGGGCAGCCGTTAGGAAA-3'; reverse, 5'-GCGCCCAATACGACCAAATC-3').

Cell counting Kit 8 (CCK-8) Assay

A CCK-8 kit (CA1210, Solarbio, China) was used to assess the viability of transfected MCF-7/MDA-MB-231 cells. Cells (5×10^3 cells/well) were seeded in 96-well plates and transfected for 48 h. Subsequently, 10 µL of CCK-8 solution was added to each well and incubated for 4 h at 37 °C. The optical density at 450 nm was measured using a CLARIOstar Plus microplate reader (BMG Labtech, Ortenberg, USA).

Wound Healing Assay

The wound healing assay was conducted to assess the migration of transfected MCF-7/MDA-MB-231 cells. Cells (5×10^5 cells/well) were seeded in 6-well plates and cultured in DMEM containing 10% FBS until complete confluence. To inhibit cell proliferation, cells were pretreated with 10 µg/mL Mitomycin C (50-07-7; M4287, Sigma-Aldrich, St. Louis, MO, USA) for 2 h prior to scratching [28]. A consistent scratch was created using a 20 µL pipette tip. Cells were then washed with PBS and cultured in DMEM containing 1% FBS for 48 h. Cell migration was examined at 0 and 48 h under an inverted microscope (CKX53, Olympus, Tokyo, Japan) at ×100 magnification.

Transwell Assay

Cell invasion was assessed using transwell chambers with 8.0 µm pore size (CLS3464, Corning Inc., Corning, NY, USA). Briefly, the upper chambers were pre-coated with 60 µL of Matrigel (356234, Solarbio, Beijing, China). A total of 1×10^5 transfected cells suspended in serum-free DMEM were added to the upper chamber, while the lower chamber was filled with 500 µL of DMEM containing 10% FBS. After 48 h of incubation, non-invasive cells on the upper surface were removed with cotton swabs. Invasive cells on the lower surface were fixed with 4% paraformaldehyde (P1110, Solarbio, Beijing, China) for 10 min, stained with crystal violet (G1062, Solarbio, Beijing, China) for 30 min, and washed with PBS. Invasive cells were observed under a CKX53 microscope at ×250 magnification.

Tartrate-Resistant Acid Phosphatase (TRAP) Staining

Following co-culture of transfected MCF-7/MDA-MB-231 cells with RAW264.7 cells, a TRAP staining kit (PMC-AK04F, Cosmo Bio, Tokyo, Japan) was used to as-

sess the maintenance, survival and functional activity of differentiated osteoclast-like cells. Mature osteoclasts were defined as TRAP-positive cells containing three or more nuclei, and only these multinucleated cells were quantified. According to the manufacturer's instructions, the culture medium was removed, and the cells were washed with PBS. Subsequently, 50 µL of 10% neutral buffered Formalin solution (F5554, Sigma-Aldrich, St. Louis, MO, Germany) was added to each well, and the cells were fixed for 5 min at room temperature, followed by washing with deionized water (250 µL/well). The Chromogenic Substrate (1 vial) was then dissolved in Tartrate-containing Buffer (5 mL) and 50 µL of the resulting solution was added to each well and incubated for 60 min at 37 °C. The reaction was stopped by washing with deionized water. Finally, the stained cells were examined at ×200 magnification using a fluorescence microscope (BX63, Olympus, Tokyo, Japan).

Bone Absorption Assay In Vitro

Following 24-h of incubation at 37 °C, RAW264.7 cells (3×10^3 cells/well) were cultured on bovine bone slices (DT-1BON1000-96, Biolead, Beijing, China) in 96-well plates and treated with 50 ng/mL RANKL for 7 days to generate mature osteoclasts. The following day, RAW264.7 cells and transfected MCF-7/MDA-MB-231 cells were co-cultured on the bone slices for 7 days in the continuous presence of 50 ng/mL RANKL. Adherent cells were removed by mechanical agitation and sonication. Finally, resorption pits were observed using a JSM-6360LV microscope (JEOL, Tokyo, Japan), and the images were analyzed using ImageJ software 1.8.0 (National Institutes of Health, Bethesda, MD, USA).

Western Blot

Total protein was extracted using RIPA lysis buffer (E-BC-R327, Elabscience, Wuhan, China), and quantified using a BCA kit (ab102536, Abcam, Cambridge, UK). Proteins were separated on 8% SDS-PAGE gels and transferred onto PVDF membranes (abs932, Absin, Shanghai, China). The membranes were blocked with 5% skim milk (D8340, Solarbio, Beijing, China) in Tris Buffered Saline with Tween-20 (T1085, Solarbio, Beijing, China) for 2 h at room temperature. Subsequently, the membranes were incubated overnight at 4 °C with primary antibodies against STIM1 (1:1000, ab108994, 77 kDa, Abcam, Cambridge, UK), COMP (1:5000, ab260037, 82 kDa, Abcam, Cambridge, UK), Acetylated-Lysine (1:1000, #9441, 82 kDa, Cell Signaling Technology, Danvers, MA, USA) and GAPDH (1:1000, ab8245, 36 kDa, Abcam, Cambridge, UK). The membranes were then incubated with Horseradish peroxidase-conjugated anti-rabbit IgG (1:1000, ab99697, Abcam, Cambridge, UK) or anti-mouse IgG (1:2000, ab6728, Abcam, Cambridge, UK) secondary antibodies at room temperature. Protein bands were visualized using ECL reagent (FP300, ABP Biosciences, Bethesda, MD, USA) with a Tanon 5200 imaging system and quantified using ImageJ software.

Microspectrofluorometry

After transfected MCF-7/MDA-MB-231 cells were co-cultured with RAW264.7 cells for 7 days, the co-cultured cells were seeded into glass bottom dishes (35 mm, D35-10-0-N, Cellvis, Mountain View, CA, USA) and washed twice with DMEM. The cells were then incubated with fura-2-AM (S1052, Beyotime, Shanghai, China) for 40 min at room temperature, followed by washing with DMEM. Fluorescence emission at 510 nm was recorded using a BX63 fluorescence microscope (×400) with Volocity software 29 (PerkinElmer, Waltham, Waltham, MA, USA). Intermittent excitation was alternated between 340 and 380 nm using a Lambda DG-4 high-speed filter changer (Sutter, USA). The 340/380 ratio was calculated for each cell after subtracting background fluorescence from cell-free areas. The ratio values were then normalized to those of the control group (set as 1.0) for each independent experiment. For each group, at least 20 cells from 5 random fields were analyzed, and all experiments were independently repeated three times.

Statistical Analysis

GraphPad Prism 8.0 software (GraphPad Software Inc., La Jolla, CA, USA) was used for statistical analysis. Data normality was assessed using the Shapiro-Wilk test, and all data met the normality assumption. Data are presented as mean ± standard deviation. Differences among multiple groups were analyzed using one-way analysis of variance, followed by Tukey's multiple comparison test for pairwise comparisons. A value of $p < 0.05$ was considered statistically significant.

Results

HDAC11 and COMP Were Highly Expressed in BC and Their Expressions Were Positively Correlated

GEPIA was used to analyze the expression of HDAC1 through HDAC11 and COMP in BC, and the results showed that HDAC11 and COMP were highly expressed in BC (Fig. 1A,B and **Supplementary Fig. 1**, $p < 0.05$). In addition, the correlation between HDAC11 and COMP expression in BCC was analyzed using StarBase, revealing a positive correlation between HDAC11 and COMP (Fig. 1C, $r = 0.141$, p-value $= 2.71 \times 10^{-6}$). qRT-PCR results further showed that the expression levels of both HDAC11 and COMP were significantly elevated in MCF-7 and MDA-MB-231 breast cancer cells compared with normal MCF-10A mammary epithelial cells (Fig. 1D,E, $p < 0.001$), consistent with the public database analysis.

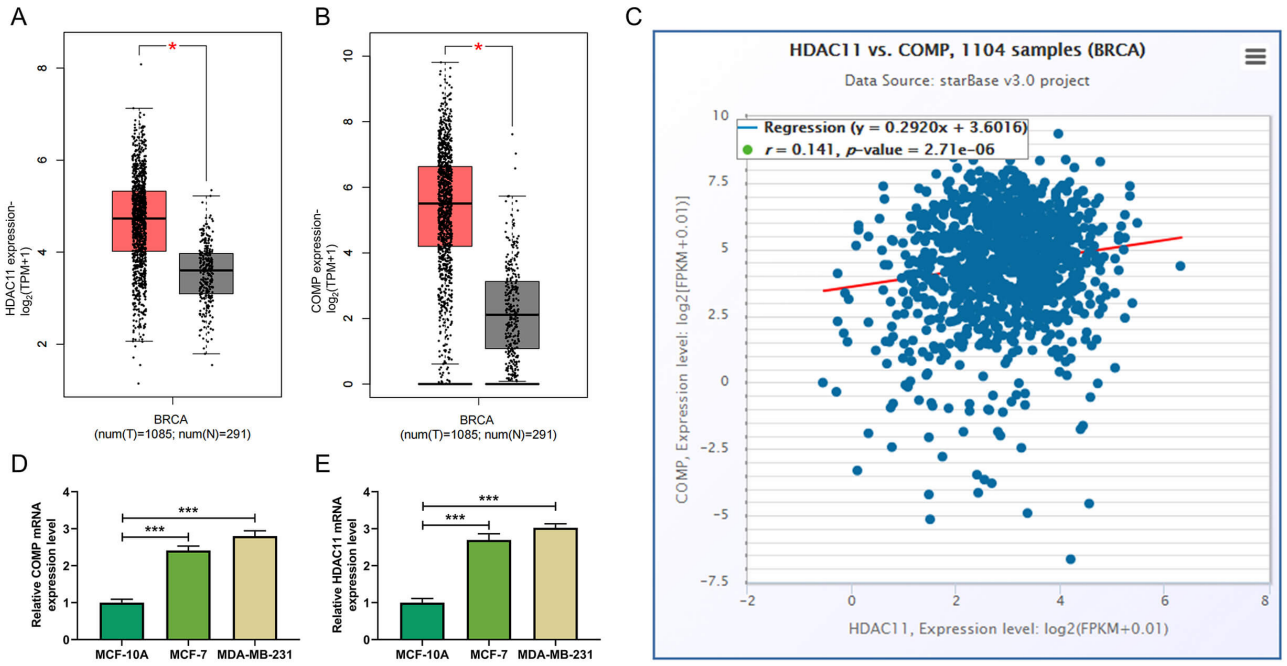

Fig. 1. Expression of HDAC11 and COMP and their correlation in BC. (A,B) HDAC11 and COMP expressions in BC. (C) Correlation between the expressions of HDAC11 and COMP in BC. (D,E) Expression levels of COMP and HDAC11 in normal breast epithelial cells (MCF-10A) and breast cancer cells (MCF-7 and MDA-MB-231) measured by qRT-PCR. Data are presented as mean ± SD (n = 3 independent experiments). $^{*}p < 0.05$, $^{***}p < 0.001$. GEPIA, gene expression profiling interactive analysis; HDAC11, histone deacetylase 11; COMP, cartilage oligomeric matrix protein; StarBase, sRNA target Base; BC, breast cancer.

Viability, Migration, Invasion, and COMP Expression in BCC Were Promoted by HDAC11 Overexpression and Suppressed by HDAC11 Knockdown

Based on the above results, HDAC11 overexpression plasmids and shHDAC11 were transfected into MCF-7/MDA-MB-231 cells, and HDAC11 expression was assessed by qRT-PCR. As shown in Fig. 2A, HDAC11 mRNA expression was decreased by shHDAC11 transfection ($p < 0.01$) and increased by the transfection of HDAC11 overexpression plasmids ($p < 0.001$) in MCF-7/MDA-MB-231 cells, confirming successful transfection. CCK-8 assay results revealed that shHDAC11 reduced MCF-7/MDA-MB-231 cell viability (Fig. 2B, $p < 0.001$), whereas HDAC11 overexpression exerted the opposite effect (Fig. 2B, $p < 0.001$). Wound-healing assay results demonstrated that shHDAC11 suppressed, whereas HDAC11 overexpression enhanced, cell migration (Fig. 2C,D, $p < 0.001$). Furthermore, as shown in Fig. 2E,F, cell invasion rate was decreased by shHDAC11($p < 0.001$), and increased by HDAC11 overexpression in MCF-7/MDA-MB-231 cells ($p < 0.01$). As shown in Fig. 2G,H, COMP protein expression was significantly decreased following shHDAC11 transfection ($p < 0.05$), whereas it was increased following HDAC11 overexpression ($p < 0.001$).

HDAC11 Knockdown Suppressed the Maintenance and Functional Activity of Differentiated Osteoclast-Like Cells, STIM1 Expression, and Fura-2 Signals

Then, MCF-7/MDA-MB-231 cells transfected with shHDAC11 were co-cultured with RAW264.7 cells for 7 days, and TRAP staining was used to assess the maintenance, survival and functional activity of differentiated osteoclast-like cells. As shown in Fig. 3A,B, osteoclast-like cells (positive staining appeared reddish purple) were increased after co-culture of shNC-transfected BCCs with RAW264.7 cells ($p < 0.001$), whereas they were decreased after co-culture of shHDAC11-transfected MCF-7/MDA-MB-231 cells with RAW264.7 cells ($p < 0.001$). In addition, STIM1 protein expression was increased after shNC-transfected MCF-7/MDA-MB-231 cells were co-cultured with RAW264.7 cells (Fig. 3C,D, $p < 0.001$), whereas it was decreased following co-culture with shHDAC11-transfected cells ($p < 0.001$). Similarly, intracellular Fura-2 signals were elevated in the co-cultured cell population, an effect that was reversed when RAW264.7 cells were co-cultured with shHDAC11-transfected cells (Fig. 3E,F, $p < 0.01$).

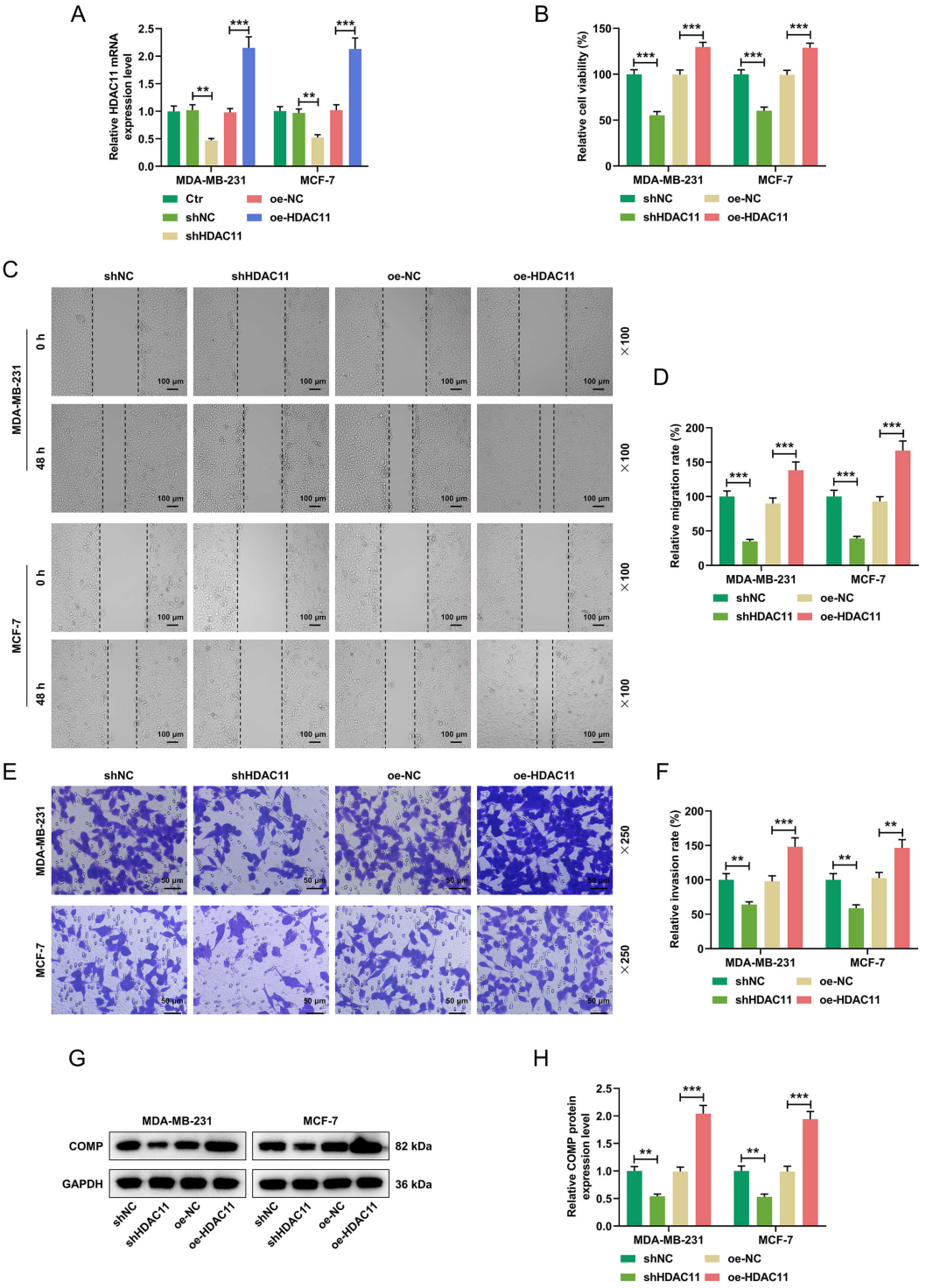

Fig. 2. Effects of HDAC11 knockdown and overexpression on viability, migration, invasion, and COMP expression in BCC. After shHDAC11 and HDAC11 overexpression plasmids were transfected into MDA-MB-231/MCF-7 cells, (A) the expression of HDAC11 was assessed by qRT-PCR (GAPDH as a loading control); (B) cell viability was tested by CCK-8 assay; (C,D) cell migration was analyzed via wound healing assay (scale: 100 μm; magnification: ×100); (E,F) cell invasion was assessed via Transwell assay (scale: 50 μm; magnification: ×250); (G,H) and the expressions of COMP in cells were evaluated by western blotting (GAPDH as a loading control). Data are presented as mean ± SD (n = 3 independent experiments). $^{**}p < 0.01$, $^{***}p < 0.001$. HDAC11, histone deacetylase 11; shHDAC11, short hairpin RNA targeting HDAC11; GAPDH, Glyceraldehyde 3-phosphate dehydrogenase; qRT-PCR, quantitative real-time reverse transcription polymerase chain reaction; CCK-8, cell counting kit 8; COMP, cartilage oligomeric matrix protein; BCC, breast cancer cells.

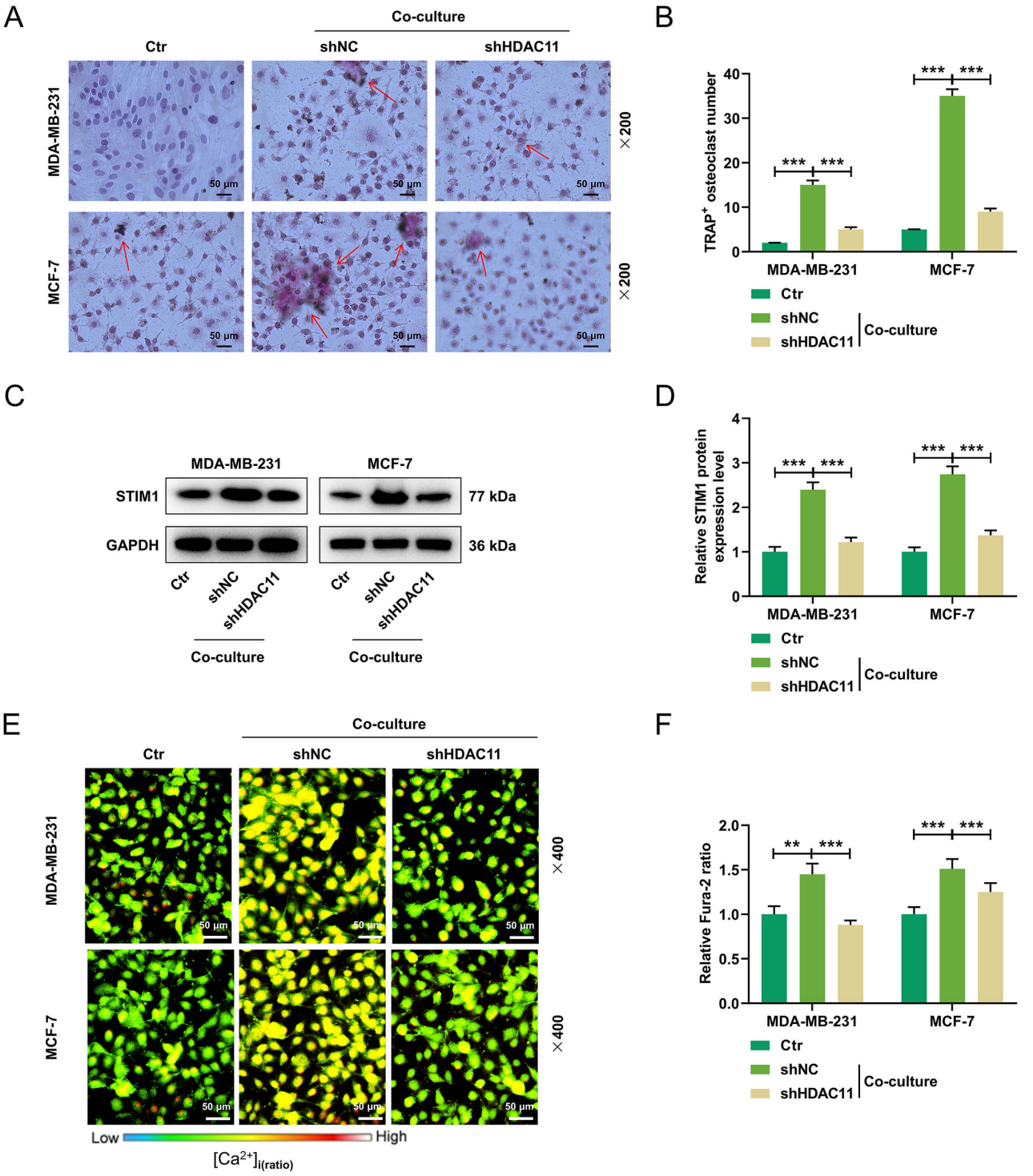

Fig. 3. Effects of HDAC11 knockdown on the maintenance and functional activity of differentiated osteoclast-like cells, STIM1 expression, and Fura-2 signals. (A–F) MCF-7 or MDA-MB-231 cells transfected with shHDAC11 were co-cultured with RAW264.7 cells for 7 days, TRAP staining (reddish purple) was used to assess the maintenance of differentiated osteoclast-like cells (A,B; scale: 50 μm; magnification: ×200), western blotting was applied to assess STIM1 expression, with GAPDH as the loading control (C,D), and microspectrofluorometry was used to measure Fura-2 signals in the co-cultured cell population (E,F; scale: 50 μm; magnification: ×400). Red arrows indicate representative osteoclasts. Data are presented as mean ± SD (n = 3 independent experiments). $^{**}p < 0.01$, $^{***}p < 0.001$. HDAC11, histone deacetylase 11; shHDAC11, short hairpin RNA targeting HDAC11; GAPDH, Glyceraldehyde 3-phosphate dehydrogenase; TRAP, tartrate-resistant acid phosphatase; STIM1, Stromal interaction molecule 1.

HDAC11 Knockdown Increased COMP Acetylation, and COMP Overexpression Attenuated the Inhibitory Effects of shHDAC11 on BCC Viability, Migration, and Invasion

The subsequent Co-IP assay demonstrated an association between HDAC11 and COMP, as evidenced by the enrichment of HDAC11/COMP following immunoprecipitation with antibodies against COMP/HDAC11 (Fig. 4A). We then examined whether HDAC11 knockdown affected COMP acetylation. As depicted in Fig. 4B, acetylated lysine signals in COMP immunoprecipitates were enhanced following HDAC11 knockdown. Subsequently, COMP overexpression plasmids were successfully transfected into MCF-7/MDA-MB-231 cells, as confirmed by the upregulation of COMP expression (Fig. 4C, $p < 0.001$). The results in Fig. 4D–H showed that the viability, migration, and invasion of MCF-7/MDA-MB-231 cells were inhibited following shHDAC11 transfection ($p < 0.01$), and these effects were reversed by COMP overexpression ($p < 0.01$). In addition, COMP overexpression promoted these phenotypes, whereas the effects were reversed by shHDAC11 (Fig. 4D–H, $p < 0.01$).

COMP Overexpression Promoted the Maintenance, Survival and Functional Activity of Differentiated Osteoclast-Like Cells, Bone Resorption, STIM1 Expression, and Fura-2 Signals, Which Were Reversed by shHDAC11

After MCF-7/MDA-MB-231 cells transfected with shHDAC11 and/or COMP overexpression plasmids were co-cultured with RAW264.7 cells, TRAP staining was performed to assess the maintenance, survival and functional activity of differentiated osteoclast-like cells. As shown in Fig. 5A,B, shHDAC11 transfection significantly decreased the number of osteoclast-like cells. ($p < 0.05$), whereas COMP overexpression markedly increased their number ($p < 0.001$). More importantly, when cells were co-transfected with shHDAC11 and the COMP overexpression plasmid and co-cultured with RAW264.7 cells, the number of osteoclast-like cells was lower than that in cells co-transfected with shNC and the COMP overexpression plasmids ($p < 0.001$), but higher than that in cells co-transfected with shHDAC11 and NC (Fig. 5A,B, $p < 0.001$). As shown in Fig. 5C–F, the bone resorption pit area and STIM1 expression were reduced following co-culture of shHDAC11-transfected MCF-7/MDA-MB-231 cells with RAW264.7 cells ($p < 0.01$), and these effects were counteracted by COMP overexpression ($p < 0.01$). As expected, bone resorption pit area and STIM1 expression were increased after co-culture of COMP-overexpressing MCF-7/MDA-MB-231 cells with RAW264.7 cells (Fig. 5C–F, $p < 0.01$), and these effects were reversed by further transfected with shHDAC11 (Fig. 5C–F, $p < 0.01$).

In addition, Fura-2 signals were reduced after co-culture of shHDAC11-transfected MCF-7/MDA-MB-231 cells with RAW264.7 cells, and this effect was reversed by COMP overexpression (Fig. 5G,H, $p < 0.001$). In the co-cultured system, COMP overexpression also increased Fura-2 signals, whereas this effect was attenuated by shHDAC11 (Fig. 5G,H, $p < 0.001$).

Discussion

Bone metastasis represents a severe complication of advanced BC and constitutes a major health threat to women worldwide, thus remaining a major focus of research [29,30]. According to previous studies, BCCs and osteoclasts engage in reciprocal cross-talk within the bone microenvironment, forming a vicious cycle and further promotes bone metastasis in BC [6,7]. Therefore, targeting osteoclasts to disrupt the vicious cycle represents a potential strategy for preventing bone metastasis. In the current study, we identified a correlative relationship that was associated with the BCC phenotypes and osteoclastogenic responses *in vitro*, which may be relevant to BC bone metastasis. This finding also distinguishes the present study from previous related research.

Osteoclasts are key bone cells responsible for the resorption of old bone [31,32], and osteoclast-mediated bone resorption is closely associated with the maintenance of bone mass [33]. Reportedly, the Ca^{2+} signaling pathway plays a pivotal role in regulating osteoclast differentiation and function [34], indicating that osteoclast viability can be effectively regulated through blockade of Ca^{2+} signaling [35]. Additionally, SOCE is considered a ubiquitous mechanism for Ca^{2+} signal generation and the maintenance of cellular homeostasis [36]. SOCE is generally regarded as a Ca^{2+} influx pathway that is activated by Ca^{2+} depletion from the endoplasmic reticulum (ER) [37]. Importantly, as a sarcoplasmic reticulum (SR) transmembrane protein, STIM1 is involved in SOCE and actively contributes to Ca^{2+} homeostasis [38]. Accordingly, we further investigated the potential role of STIM1 in bone metastasis of BC. Interestingly, previous studies have reported high expression of COMP, a STIM1-interacting protein, in the blood of patients with BC [19,20]. Consistently, our results showed increased STIM1 expression in the co-cultured cell population, supporting its potential involvement in BC-associated bone metastasis.

Moreover, the role of COMP in BC also attracted our attention. Histone acetylation modifications are regulated by HDACs and histone acetyltransferases (HAT) and have been shown to substantially affect the functions of various cell types [21,22]. Previous evidence has revealed that HDAC3 inhibits COMP acetylation [24], while COMP expression is markedly suppressed by HDAC1 and HDAC2 overexpression in human articular chondrocytes [24]. Herein, analysis of various HDACs in BC using GEPIA revealed that HDAC11 was significantly upregulated in tumor tissues. Therefore, in the current study, we

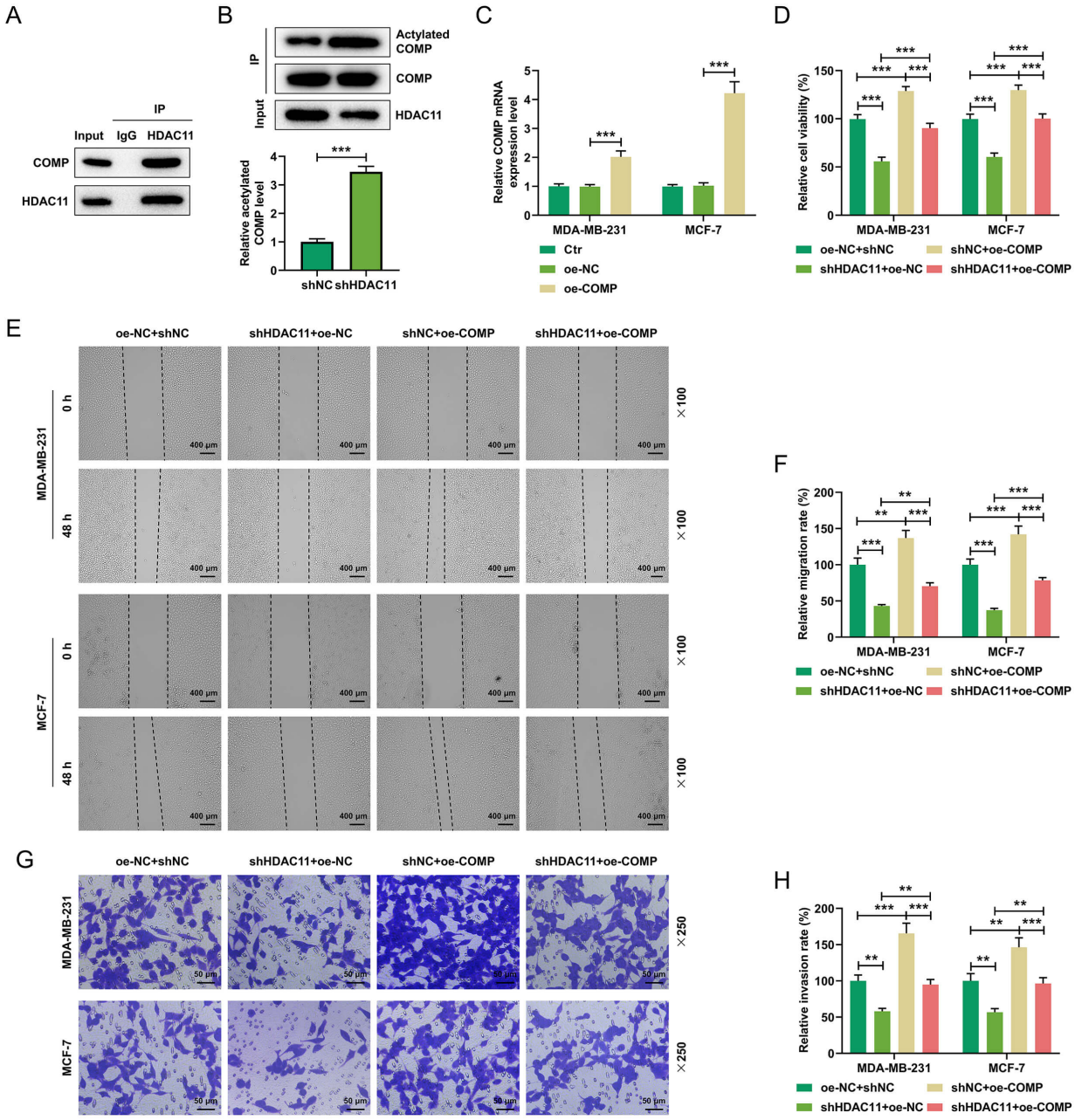

Fig. 4. Effects of shHDAC11 and COMP overexpression on viability, migration and invasion of BCC. (A) The mutual interaction between HDAC11 and COMP was evaluated by Co-IP assay. (B) *In vitro* acetylation assay was performed to measure acetylated-lysine signals in COMP immunoprecipitates following HDAC11 knockdown. (C) COMP overexpression plasmids were transfected into MCF-7/MDA-MB-231 cells, and COMP expression was analyzed by qRT-PCR with GAPDH as the loading control. (D–H) After MCF-7/MDA-MB-231 cells were transfected with shHDAC11 and COMP overexpression plasmids, cell viability was assessed by CCK-8 assay (D), cell migration was evaluated by wound healing assay (E,F; scale: 100 μm; magnification: ×100), and cell invasion was analyzed by Transwell assay (G,H; scale: 50 μm; magnification: ×250). Data are presented as mean ± SD (n = 3 independent experiments). $^{**}p < 0.01$, $^{***}p < 0.001$. BCC, breast cancer cells; HDAC11, histone deacetylase 11; shHDAC11, short hairpin RNA targeting HDAC11; GAPDH, Glyceraldehyde 3-phosphate dehydrogenase; COMP, cartilage oligomeric matrix protein; qRT-PCR, quantitative real-time reverse transcription polymerase chain reaction; CCK-8, cell counting kit 8; Co-IP, Co-immunoprecipitation.

focused on HDAC11 and COMP/STIM1. We confirmed the upregulation and positive correlation of HDAC11 and COMP in invasive BC, indicating their potential association with BC progression. Furthermore, BCC viability, migration, invasion, and COMP expression were promoted by HDAC11 overexpression and suppressed by HDAC11 si-

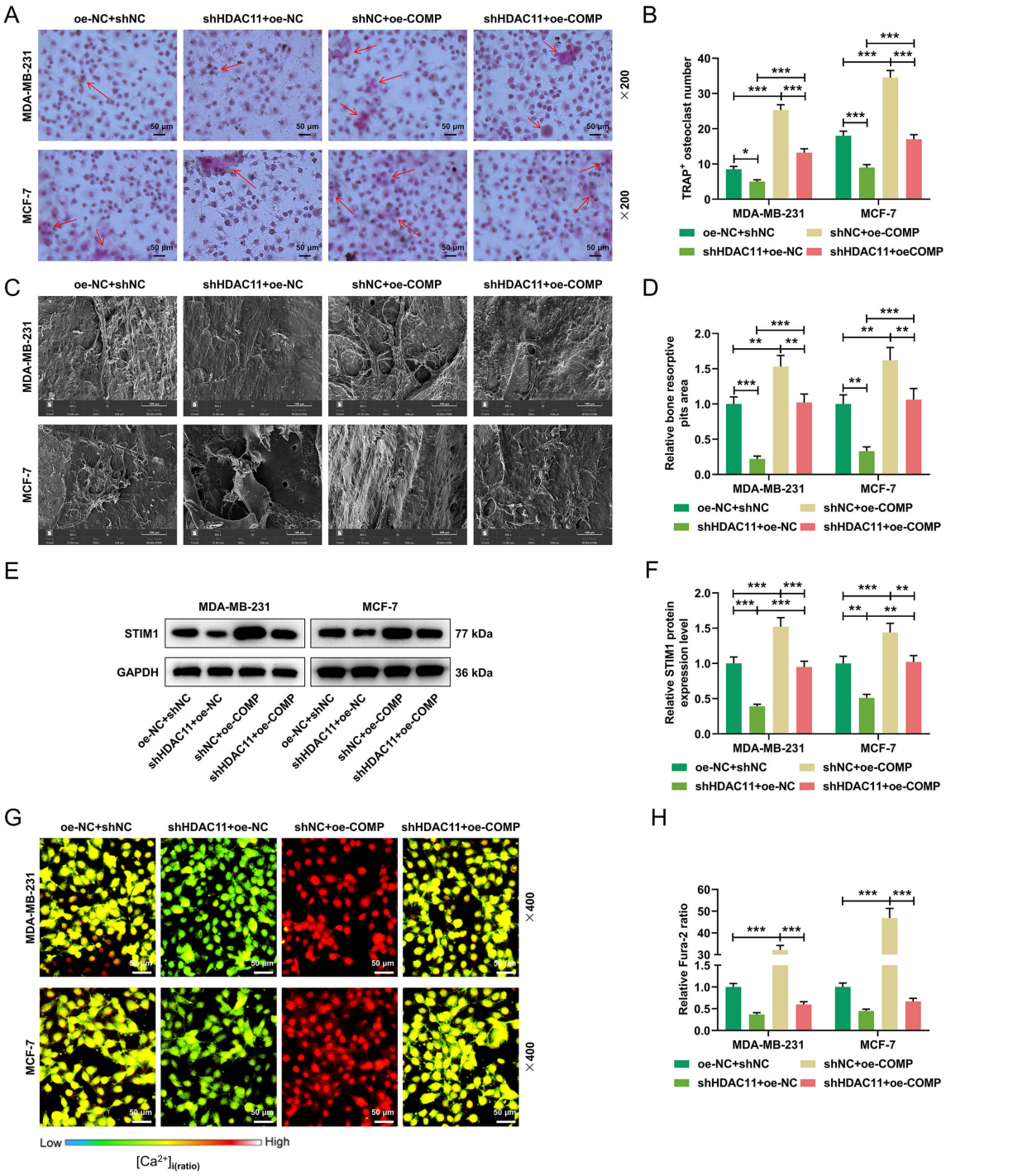

Fig. 5. Effects of HDAC11 knockdown and COMP overexpression on the maintenance, survival and functional activity of differentiated osteoclast-like cells, bone resorption, STIM1 expression, and Fura-2 signals. (A–G) After MCF-7 or MDA-MB-231 cells transfected with shHDAC11 and/or COMP overexpression plasmids were co-cultured with RAW264.7 cells, TRAP staining (reddish purple) was used to assess the maintenance, survival and functional activity of differentiated osteoclast-like cells (A,B; scale: 50 μm; magnification: ×200), a bone resorption assay was used to evaluate osteoclast-like cell-mediated bone resorption (C,D), western blotting was performed to quantify STIM1 expression with GAPDH as the loading control (E,F), and microspectrofluorometry was used to measure Fura-2 signals in the co-cultured cell population (G,H; scale: 50 μm; magnification: ×400). Red arrows indicate representative osteoclasts. Data are presented as mean ± SD (n = 3 independent experiments). $^{*}p < 0.05$, $^{**}p < 0.01$, $^{***}p < 0.001$. HDAC11, histone deacetylase 11; shHDAC11, short hairpin RNA targeting HDAC11; GAPDH, Glyceraldehyde 3-phosphate dehydrogenase; COMP, cartilage oligomeric matrix protein; TRAP, tartrate-resistant acid phosphatase; STIM1, Stromal interaction molecule 1.

lencing. Notably, HDAC3 (Class I) and HDAC11 (Class IV) are distinct HDAC family members with different subcellular localizations and substrate preferences. The observation that both HDAC3 and HDAC11 are associated with COMP acetylation suggests that COMP acetylation may be regulated by multiple HDACs in a context-dependent manner. The potential redundancy or specificity of these HDACs in BC bone metastasis warrants further investigation.

With respect to bone metastasis, TRAP is commonly considered a marker of osteoclasts [39]. Accumulating evidence has demonstrated that osteoclasts can interact with BCCs to enhance cancer cell proliferation while increasing bone resorption [40]. Moreover, limiting osteoclast-mediated bone resorption has been shown to effectively reduce tumor-driven osteolysis [31,32]. Consistent with previous studies, we observed that HDAC11 silencing suppressed the maintenance, survival and functional activity of differentiated osteoclast-like cells, as well as bone resorption. We further confirmed that HDAC11 silencing reduced STIM1 expression and calcium influx, providing additional evidence for its inhibitory effect on bone metastasis. Therefore, these findings suggest an association between HDAC11 and the regulation of BC-associated bone metastasis, as well as between HDAC11 knockdown and increased COMP acetylation.

Subsequent studies are necessary to address the current limitations in several aspects. *In vivo* BC bone metastasis models should be established to validate the therapeutic potential of targeting the HDAC11/COMP/STIM1 association. Additionally, whether human COMP directly acts on mouse STIM1 remains to be verified. The generalizability of our findings should be further confirmed by expanding the analysis to additional BC subtypes and patient-derived samples. The crosstalk between HDAC11 and other HDAC family members in regulating COMP acetylation and BC bone metastasis also requires further investigations to facilitate the development of optimized therapeutic strategies. Moreover, future studies using dedicated clinical cohorts are warranted to validate the prognostic value of HDAC11 and COMP in BC bone metastasis. Although bioinformatics analysis revealed higher HDAC11 and COMP expression in BC tissues, their associations with bone metastasis-specific patient survival were not analyzed. Finally, this study primarily focused on the maintenance, survival, and functional activity of differentiated osteoclast-like cells and bone resorption, but did not directly evaluate whether HDAC11 knockdown or COMP overexpression affects osteoclast survival or apoptosis, which warrants further investigation using assays such as TUNEL staining or caspase-3 activity measurements.

Conclusion

In summary, our study provides initial evidence that HDAC11 is associated with the regulation of COMP-related STIM1 protein abundance and Fura-2 signals in the co-culture system, which correlates with both BCC malignant progression and osteoclast-mediated bone resorption. These findings suggest a potential epigenetic and signaling link that may contribute to BC bone metastasis and provide a basis for future *in vivo* studies to further investigate its functional significance.

Availability of Data and Materials

The datasets used or analyzed during the current study are available from the corresponding author upon reasonable request.

Author Contributions

XHY: Conceptualization, Methodology, Validation, Writing - original draft, Writing review & editing. PW: Conceptualization, Formal analysis, Validation, Writing - original draft, Writing review & editing. YP: Data curation, Formal analysis, Methodology, Writing - original draft, Writing review & editing. GL: Investigation, Visualization, Supervision, Writing- original draft, Writing review & editing. YZ: Data curation, Formal analysis, Investigation, Writing - original draft, Writing review & editing. All authors gave final approval of the version to be published. All authors have participated sufficiently in the work to take public responsibility for appropriate portions of the content and agreed to be accountable for all aspects of the work in ensuring that questions related to its accuracy or integrity.

Ethics Approval and Consent to Participate

Not applicable.

Acknowledgment

Not applicable.

Funding

This work was supported by the Nanjing Municipal Health Commission [grant number: YKK23250].

Conflict of Interest

The authors declare no conflict of interest.

Supplementary Material

Supplementary material associated with this article can be found, in the online version, at https://doi.org/10.24976/Discov.Med.202638212.220.

References

[1] Siegel RL, Miller KD, Fuchs HE, Jemal A. Cancer statistics, 2022. CA: a Cancer Journal for Clinicians. 2022; 72: 7–33. https://doi.org/10.3322/caac.21708

[2] Xiong X, Zheng LW, Ding Y, Chen YF, Cai YW, Wang LP, et al. Breast cancer: pathogenesis and treatments. Signal Transduction and Targeted Therapy. 2025; 10: 49. https://doi.org/10.1038/s41392-024-02108-4

[3] Jiang B, Bao L, He S, Chen X, Jin Z, Ye Y. Deep learning applications in breast cancer histopathological imaging: diagnosis, treatment, and prognosis. Breast Cancer Research : BCR. 2024; 26: 137. https://doi.org/10.1186/s13058-024-01895-6

[4] Whiteley AE, Ma D, Wang L, Yu SY, Yin C, Price TT, et al. Breast cancer exploits neural signaling pathways for bone-to-meninges metastasis. Science (New York, N.Y.). 2024; 384: eadh5548. https://doi.org/10.1126/science.adh5548

[5] Shao H, Varamini P. Breast Cancer Bone Metastasis: A Narrative Review of Emerging Targeted Drug Delivery Systems. Cells. 2022; 11: 388. https://doi.org/10.3390/cells11030388

[6] Hofbauer LC, Bozec A, Rauner M, Jakob F, Perner S, Pantel K. Novel approaches to target the microenvironment of bone metastasis. Nature Reviews. Clinical Oncology. 2021; 18: 488–505. https://doi.org/10.1038/s41571-021-00499-9

[7] Liu X, Ma R, Wei F, Wang M, Jiang Y, Zheng P, et al. Tumor-derived exosomal lncRNA-MIR193BHG promotes bone metastasis of breast cancer by targeting the miR-489-3p/DNMT3A signaling axis in osteoclasts. Journal of Translational Medicine. 2025; 23: 142. https://doi.org/10.1186/s12967-025-06156-4

[8] Ganesan K, Xu C, Wu S, Sui Y, Du B, Zhang J, et al. Ononin Inhibits Tumor Bone Metastasis and Osteoclastogenesis By Targeting Mitogen-Activated Protein Kinase Pathway in Breast Cancer. Research (Washington, D.C.). 2024; 7: 0553. https://doi.org/10.34133/research.0553

[9] Li X, Liang Y, Lian C, Peng F, Xiao Y, He Y, et al. CST6 protein and peptides inhibit breast cancer bone metastasis by suppressing CTSB activity and osteoclastogenesis. Theranostics. 2021; 11: 9821–9832. https://doi.org/10.7150/thno.62187

[10] Kaur J, Adhikari M, Sabol HM, Anloague A, Khan S, Kurihara N, et al. Single-Cell Transcriptomic Analysis Identifies Senescent Osteocytes That Trigger Bone Destruction in Breast Cancer Metastasis. Cancer Research. 2024; 84: 3936–3952. https://doi.org/10.1158/0008-5472.CAN-24-0857

[11] Sui L, Wang J, Jiang WG, Song X, Ye L. Molecular mechanism of bone metastasis in breast cancer. Frontiers in Oncology. 2024; 14: 1401113. https://doi.org/10.3389/fonc.2024.1401113

[12] Puppo M, Croset M, Ceresa D, Valluru MK, Canuas Landero VG, Hernandez Guadarrama M, et al. Protective effects of miR-24-2-5p in early stages of breast cancer bone metastasis. Breast Cancer Research : BCR. 2024; 26: 186. https://doi.org/10.1186/s13058-024-01934-2

[13] Hao Y, Yang N, Sun M, Yang S, Chen X. The role of calcium channels in osteoporosis and their therapeutic potential. Frontiers in Endocrinology. 2024; 15: 1450328. https://doi.org/10.3389/fendo.2024.1450328

[14] Chanaday NL, Nosyreva E, Shin OH, Zhang H, Aklan I, Atasoy D, et al. Presynaptic store-operated Ca^{2+} entry drives excitatory spontaneous neurotransmission and augments endoplasmic reticulum stress. Neuron. 2021; 109: 1314–1332.e5. https://doi.org/10.1016/j.neuron.2021.02.023

[15] Martínez-Carrasco R, Fini ME. Dynasore modulates store-operated calcium entry and mitochondrial calcium release in corneal epithelial cells. Experimental Eye Research. 2024; 247: 110029. https://doi.org/10.1016/j.exer.2024.110029

[16] Rubaiy HN. ORAI Calcium Channels: Regulation, Function, Pharmacology, and Therapeutic Targets. Pharmaceuticals (Basel, Switzerland). 2023; 16: 162. https://doi.org/10.3390/ph16020162

[17] Benson JC, Trebak M. Too much of a good thing: The case of SOCE in cellular apoptosis. Cell Calcium. 2023; 111: 102716. https://doi.org/10.1016/j.ceca.2023.102716

[18] Wang YH, Li W, McDermott M, Son GY, Maiti G, Zhou F, et al. IFN-γ-producing T_H1 cells and dysfunctional regulatory T cells contribute to the pathogenesis of Sjögren's disease. Science Translational Medicine. 2024; 16: eado4856. https://doi.org/10.1126/scitranslmed.ado4856

[19] Yao F, Yan C, Zhang Y, Shen L, Zhou D, Ni J. Identification of blood protein biomarkers for breast cancer staging by integrative transcriptome and proteome analyses. Journal of Proteomics. 2021; 230: 103991. https://doi.org/10.1016/j.jprot.2020.103991

[20] Jafari N, Kolla M, Meshulam T, Shafran JS, Qiu Y, Casey AN, et al. Adipocyte-derived exosomes may promote breast cancer progression in type 2 diabetes. Science Signaling. 2021; 14: eabj2807. https://doi.org/10.1126/scisignal.abj2807

[21] Sun X, Shu Y, Ye G, Wu C, Xu M, Gao R, et al. Histone deacetylase inhibitors inhibit cervical cancer growth through Parkin acetylation-mediated mitophagy. Acta Pharmaceutica Sinica. B. 2022; 12: 838–852. https://doi.org/10.1016/j.apsb.2021.07.003

[22] Ibrahim HS, Sippl W. Histone Acetyltransferase and Deacetylase Inhibitors-New Aspects and Developments. International Journal of Molecular Sciences. 2023; 24: 16985. https://doi.org/10.3390/ijms242316985

[23] Liu F, He L, Yu M, Chen J, Huang Y, Ma W, et al. Histone Modification Networks Reshape the Metabolism and Treatment Landscape of Urological Cancers. Frontiers in Bioscience (Landmark Edition). 2025; 30: 42831. https://doi.org/10.31083/FBL42831

[24] Hridayanka KSN, Duttaroy AK, Basak S. Bioactive Compounds and Their Chondroprotective Effects for Osteoarthritis Amelioration: A Focus on Nanotherapeutic Strategies, Epigenetic Modifications, and Gut Microbiota. Nutrients. 2024; 16: 3587. https://doi.org/10.3390/nu16213587

[25] Graf LG, Vogt R, Blasl AT, Qin C, Schulze S, Zühlke D, et al. Assays to Study Enzymatic and Non-Enzymatic Protein Lysine Acetylation In Vitro. Current Protocols. 2021; 1: e277. https://doi.org/10.1002/cpz1.277

[26] Li T, Jiang G, Hu X, Yang D, Tan T, Gao Z, et al. Punicalin Attenuates Breast Cancer-Associated Osteolysis by Inhibiting the NF-κB Signaling Pathway of Osteoclasts. Frontiers in Pharmacology. 2021; 12: 789552. https://doi.org/10.3389/fphar.2021.789552

[27] Su Y, Wang Y, Yu Q, Wu Z, Zhang D, Yan C. Eugenol suppresses VEGF-dependent angiogenesis by JAK2/STAT3 pathway in non-small cell lung cancer. Guidelines and Standards of Chinese Medicine. 2024; 2: 80–90. https://doi.org/10.1097/gscm.0000000000000021

[28] Huang J, Ding J, Wang Z, Li Y, He Y, Wang X, et al. Icariside II Attenuates Methamphetamine-Induced Neurotoxicity and Behavioral Impairments via Activating the Keap1-Nrf2 Pathway. Oxidative Medicine and Cellular Longevity. 2022; 2022: 8400876. https://doi.org/10.1155/2022/8400876

[29] Song X, Wei C, Li X. The Signaling Pathways Associated With Breast Cancer Bone Metastasis. Frontiers in Oncology. 2022; 12: 855609. https://doi.org/10.3389/fonc.2022.855609

[30] Zhang X, Zhang Y, Du W. Alleviating role of ketamine in breast cancer cell-induced osteoclastogenesis and tumor bone metastasis-induced bone cancer pain through an SRC/EGR1/CST6 axis. BMC Cancer. 2024; 24: 1535. https://doi.org/10.1186/s12885-024-13290-7

[31] Li KX, Sun X, Li BY, Yokota H. Conversion of Osteoclasts into Bone-Protective, Tumor-Suppressing Cells. Cancers. 2021; 13: 5593. https://doi.org/10.3390/cancers13225593

[32] Veis DJ, O'Brien CA. Osteoclasts, Master Sculptors of Bone. Annual Review of Pathology. 2023; 18: 257–281. https://doi.or

g/10.1146/annurev-pathmechdis-031521-040919

[33] Lu J, He Q, Wang H, Yao L, Duffy M, Guo H, et al. Bone marrow adipogenic lineage precursors are the major regulator of bone resorption in adult mice. Bone Research. 2025; 13: 39. https://doi.org/10.1038/s41413-025-00405-4

[34] Zhu Y, Meng X, Zhai Q, Xin L, Tan H, He X, et al. Heavy mechanical force decelerates orthodontic tooth movement via Piezo1-induced mitochondrial calcium down-regulation. Genes & Diseases. 2025; 12: 101434. https://doi.org/10.1016/j.gendis.2024.101434

[35] Kim HJ, Lee J, Lee GR, Kim N, Lee HI, Kwon M, et al. Flunarizine inhibits osteoclastogenesis by regulating calcium signaling and promotes osteogenesis. Journal of Cellular Physiology. 2021; 236: 8239–8252. https://doi.org/10.1002/jcp.30496

[36] Lu F, Li Y, Lin S, Cheng H, Yang S. Spatiotemporal regulation of store-operated calcium entry in cancer metastasis. Biochemical Society Transactions. 2021; 49: 2581–2589. https://doi.org/10.1042/BST20210307

[37] Umemura M, Nakakaji R, Ishikawa Y. Physiological functions of calcium signaling via Orai1 in cancer. The Journal of Physiological Sciences : JPS. 2023; 73: 21. https://doi.org/10.1186/s12576-023-00878-0

[38] Zhang H, Bryson VG, Wang C, Li T, Kerr JP, Wilson R, et al. Desmin interacts with STIM1 and coordinates Ca2+ signaling in skeletal muscle. JCI Insight. 2021; 6: e143472. https://doi.org/10.1172/jci.insight.143472

[39] Yuan H, Bao Y, Li L, Luan Y, Li F. A novel HDAC1-specific inhibitor prevents estrogen deficiency-induced osteoporosis in mice by inhibiting osteoclast function. Archives of Gerontology and Geriatrics. 2025; 139: 106020. https://doi.org/10.1016/j.archger.2025.106020

[40] Inson I, Chutoe C, Kanjanapipak J, Lertsuwan K. Cannabinoid Receptor Type 2 Agonist, GW405833, Reduced the Impacts of MDA-MB-231 Breast Cancer Cells on Bone Cells. Cancer Medicine. 2025; 14: e70709. https://doi.org/10.1002/cam4.70709